Journal of Zhejiang University-SCIENCE A in press
www.jzus.zju.edu.cn; www.springer.com/journal/11582
E-mail: jzus_a@zju.edu.cn

Research Article
https://doi.org/10.1631/jzus.A2500621

Unveiling the drivers of $PM_{2.5}$ and O_3 pollution rebound in Shandong, China during three periods of 2023 by an integrated machine learning method

Gang WANG[1], Sai LIU[1], Kai WANG[2,3], Huijuan MENG[4], Na ZHAO[5]✉, Hanyu ZHANG[6]✉

[1]*Department of Environmental and Safety Engineering, College of Chemistry and Chemical Engineering, China University of Petroleum (East China), Qingdao 266580, China*
[2]*Shandong Academy for Environmental Planning, Jinan 250101, China*
[3]*Key Laboratory of Land and Sea Ecological Governance and Systematic Regulation, Ministry of Ecology and Environment, Jinan 250101, China*
[4]*Engineering Training Management Center, Jinan Engineering Polytechnic, Jinan 250200, China*
[5]*Environment Research Institute, Shandong University, Qingdao 266237, China*
[6]*Department of Environmental Science and Engineering, Beijing Technology and Business University, Beijing 100048, China*

Abstract: Following the relaxation of coronavirus disease 2019 restrictions and the subsequent full economic recovery, Shandong Province experienced a 4.3% rebound in the air quality index in 2023, with both fine particulate matter ($PM_{2.5}$) and ozone (O_3) concentrations exhibiting noticeable upward trends. Quantifying the drivers of this rebound is essential for developing targeted air quality management strategies. To this end, the analysis focused on the early spring period (ESP, February–April) and autumn harvest period (AHP, September–October) for $PM_{2.5}$ pollution and the photochemical season period (PSP, July–October) for O_3 pollution. We developed an interpretable random forest–Shapley additive explanation (RF–SHAP) framework optimized with a tree-structured Parzen estimator (TPE) to assess the impacts of anthropogenic emissions and meteorological factors. The introduction of the TPE optimization technique enhanced RF model performance across these pollution periods. Anthropogenic emissions played the dominant role in $PM_{2.5}$ pollution rebounds, contributing 14.1% during the ESP and 19.0% during the AHP, for example, industrial recovery (9.2% increase in energy consumption) and agricultural waste burning (70.0% increase in crop residue burning incident). In contrast, O_3 pollution was more strongly influenced by meteorological conditions, which contributed a 5.8% increase during the PSP. Critical meteorological drivers included strengthened atmospheric oxidation capacity, reduced total cloud cover, and changes in boundary layer height, although precursor emissions from the transportation and petrochemical industries remained indispensable for O_3 formation. This study provides an important scientific basis for precise air quality management in Shandong Province in the postpandemic period.

Key words: Air pollution rebound; Driving factors; Random forest–Shapley additive explanation (RF–SHAP); Anthropogenic emissions; Meteorological conditions

1 Introduction

In recent years, China has made remarkable progress in air quality improvement, particularly in controlling fine particulate matter ($PM_{2.5}$) pollution (Li et al., 2019; Hou et al., 2025; Wen et al., 2024; Zhao et al., 2025). However, with the gradual relaxation of coronavirus disease 2019 (COVID-19) prevention and control measures and rapid socioeconomic recovery in 2023, air quality deterioration was observed in some regions (MEE, 2024; Song et al., 2025), with Shandong Province being particularly affected. As a crucial economic and industrial hub in eastern China, Shandong Province recorded an average comprehensive air quality index of 4.35 in 2023, representing a 4.3% rebound compared to 2022 (SPPG, 2024a). Notably, both $PM_{2.5}$ and ozone (O_3) concentrations showed significant increasing trends in 2023, increasing by

✉ Na ZHAO, zhaona2023@sdu.edu.cn
Hanyu ZHANG, zhy@btbu.edu.cn
Hanyu ZHANG, https://orcid.org/0009-0000-7135-4197

Received Dec. 6, 2025; Revision accepted Apr. 23, 2026;
Crosschecked

3.8% and 2.8%, respectively (SPPG, 2024b). This pollution rebound not only poses potential threats to public health but also presents new challenges for regional air quality management.

Air pollutant concentrations are influenced by both anthropogenic emissions and meteorological conditions (Chen et al., 2025; Dai et al., 2023; Wang et al., 2025). Anthropogenic emissions, particularly from industrial production, transportation networks, and fossil fuel-based energy generation systems, constitute the dominant anthropogenic sources of primary air pollutants and precursors of secondary pollutants (Levi et al., 2024; Merico et al., 2020; Nizamani et al., 2024; Shen et al., 2019). Accelerated economic development and urban sprawl have led to substantial increases in energy consumption and industrial activity, consequently elevating emissions of various air pollutants (Li et al., 2023). Meanwhile, meteorological conditions play a crucial modulating role in air quality by governing atmospheric processes that affect pollutant behavior (Pendergrass et al., 2025). For example, wind speed and direction control the dispersion of pollutants (Zhang et al., 2024). Temperature, humidity, atmospheric oxidizing potential, and solar radiation affect the photochemical reaction rates of precursors (Zhang et al., 2025a). Existing studies suggest that post-COVID economic recovery may lead to significant increases in pollutant emissions (Madukpe et al., 2025; MEE, 2024; Song et al., 2025), although interannual variations in meteorological conditions should not be overlooked. However, current research on the drivers and relative contributions of the 2023 $PM_{2.5}$ and O_3 rebound in Shandong Province remains limited, highlighting the need for systematic quantification of anthropogenic and meteorological impacts to inform evidence-based pollution control strategies.

In recent years, chemical transport models (CTMs) have played an important role in air quality assessment (Assareh et al., 2025; Xiao et al., 2021). Among these, the Weather Research and Forecasting-Community Multiscale Air Quality Modeling System was applied by Zhang et al. (2019) to analyze the factors influencing changes in $PM_{2.5}$ concentrations in China from 2013 to 2017, concluding that anthropogenic emissions were the key factor driving improvements in air quality. However, the accuracy of such models is significantly constrained by the reliability and timeliness of emission inventories (Kim et al., 2025; Liu et al., 2025c). Receptor models provide a complementary approach for source apportionment without relying on emission inventories (Belis et al., 2020). However, unlike CTMs, they do not explicitly account for meteorological conditions and thus cannot disentangle the effects of anthropogenic emissions from meteorological variability. With the development of machine learning (ML) technology, its application in atmospheric research has become increasingly widespread. Compared to traditional statistical analysis methods and CTMs, ML models demonstrate superior performance in $PM_{2.5}$ concentration prediction (Jia et al., 2026; Jiang & Ma, 2025; Shi et al., 2021). Liu et al. (2022) used a random forest (RF) model to conduct a quantitative analysis of $PM_{2.5}$ concentration changes during the COVID-19 pandemic in Hubei Province. The results showed that the reduction in anthropogenic emissions led to a significant 33.3% decrease in $PM_{2.5}$ concentrations, while unfavorable meteorological conditions caused $PM_{2.5}$ concentrations to rise by 8.8%. Elbir et al. (2025) found that the LightGBM model effectively predicted $PM_{2.5}$ concentrations in the Marmara region, with boundary layer height identified as a key predictor. Hou et al. (2022) further combined the random forest model with the Shapley additive explanation (SHAP) algorithm to deeply analyze the formation mechanisms of five typical haze events during China's epidemic prevention and control period and found that high emission levels were the primary driving factors behind these pollution events. Compared to other ML models, such as CatBoost and XGBoost, RF has unique advantages. As an ensemble learning algorithm, RF constructs multiple decision trees and employs bootstrap aggregation and random feature selection mechanisms to effectively handle nonlinear relationships between predictive variables and pollutants while avoiding model overfitting (Li & Sun, 2024). However, the “black box” nature of ML models limits the physical interpretability of their results. To address this, we employed the game theory-based SHAP explanation framework, which quantifies the contribution of each feature to the prediction results by calculating their Shapley values, thereby enhancing the interpretability of ML models

(Lundberg & Lee, 2017; Mangalathu et al., 2020; Yao et al., 2025b). Given that the SHAP algorithm derives its interpretability from underlying ML model performance, rigorous optimization of the model is essential. To achieve this, we integrated the tree-structured Parzen estimator (TPE) sampling algorithm based on the Optuna framework for hyperparameter optimization to improve model performance (Zhang et al., 2025c).

This study focuses on Shandong Province and integrates air quality monitoring data from 2022–2023, meteorological reanalysis data, and an interpretable ML framework that combines random forest with the SHAP algorithm to systematically quantify the contributions of anthropogenic emissions and meteorological factors to the $PM_{2.5}$ and O_3 pollution rebounds observed in 2023. To further enhance model performance, the RF–SHAP framework was optimized using TPE techniques.

The analysis targets three critical pollution periods: the early spring period (February to April), the photochemical season (July to October), and the autumn harvest period (September to October), with the aim of identifying the dominant drivers responsible for pollution rebounds across different seasons. The findings improve the understanding of the mechanisms underlying air pollution in Shandong Province and support coordinated strategies for air-quality improvement and green economic recovery in the postpandemic era.

2 Methods

2.1 Study region

Shandong Province is situated on the eastern coast of China and the lower reaches of the Yellow River. The region is centered around the Taishan Mountains (elevation 1,545 meters), with the North China Plain to the west and north and the Jiaodong Peninsula to the east, characterized by a warm temperate monsoon climate. Shandong Province is a pivotal economic and demographic center of the country. As of 2023, it hosted a permanent resident population of 102 million, with an urbanization rate of 64.3%. The province comprises 16 prefecture-level cities, 136 county-level administrative divisions, and 1,825 towns. With a robust economy, Shandong Province ranked third in China's provincial gross domestic product (GDP) rankings in 2023, achieving a regional GDP of 9.2 trillion RMB, a year-on-year increase of 6.0% (SDBS, 2024). Its industrial system covers 41 major categories of the national economy, supported by three pillar industries: petrochemicals, steel, and equipment manufacturing. The province boasts advanced infrastructure, including a road density of 1.76 km/km^2, an annual port throughput of 1.97 billion tons (MOT, 2024), and 30 million motor vehicles. These attributes make Shandong an exemplary region for investigating the formation mechanisms of regional air pollution.

2.2 Online data sources and processing

Hourly air quality monitoring data for $PM_{2.5}$, O_3, sulfur dioxide (SO_2), and nitrogen dioxide (NO_2) during 2022–2023 were collected from 106 national-level environmental monitoring stations across Shandong Province (https://data.epmap.org/page/index). All monitoring instruments were certified by China's Ministry of Ecology and Environment (MEE) and operated in strict compliance with the national standard HJ 818-2018 for continuous automated monitoring of gaseous pollutants. The dataset exhibited 99.0% completeness, with missing values excluded from analysis to ensure data reliability. For O_3 pollution evaluation, the daily maximum 8-hour average concentration (MDA8-O_3) served as the daily metric, while monthly assessments were based on the mean MDA8-O_3 values. Chemical compositions, including SO_4^{2-}, NO_3^-, NH_4^+, organic matter (OM), and black carbon (BC), across data in Shandong Province were obtained from the Tracking Air Pollution (TAP, http://tapdata.org). The measured gaseous pollutants and chemical components are used as supporting data for changes in emission and secondary formation analysis.

Hourly meteorological data, including wind speed at 10 m height (WS), relative humidity at 2 m (RH), temperature at 2 m (T), surface pressure (SP), total precipitation (TP), boundary layer height (BLH), surface net solar radiation (SSRD), and total cloud cover (TCC), were obtained from the Fifth Generation of ECMWF Atmospheric Reanalysis (ERA5). The ERA5 data feature a spatial resolution of 0.25° × 0.25° and an hourly temporal resolution (https://cds.climate.copernicus.eu).

2.3 Offline sampling

To support the identified driving factors of pollution rebound, we selected Linyi in Shandong Province—known as China's plate and logistics capital—as a representative case study and conducted chemical composition analysis. Linyi is a central city in southeastern Shandong Province, strategically located at the intersection of the Yangtze River Delta Economic Zone and the Bohai Economic Rim. The city's pollution pattern features unresolved coal-smoke pollution alongside emerging O_3 issues, reflecting its ongoing transition toward the complex air pollution regime typical of many northern Chinese cities. In Linyi, atmospheric $PM_{2.5}$ component sampling was performed in February, March, April, September, and October. During the high-pollution period (February to March), $PM_{2.5}$ was sampled once daily. In April and from September to October, the sampling frequency was reduced to once every three days. Concentrations of SO_4^{2-}, NO_3^-, NH_4^+, organic carbon (OC), and elemental carbon (EC) were determined.

Photochemical Assessment Monitoring Station (PAMS) components (including alkanes, aromatics, alkenes, and alkynes) and oxygenated volatile organic compounds (OVOCs) were also sampled in Linyi using electropolished stainless-steel canisters and dinitrophenylhydrazine (DNPH) columns, respectively. Both sample types were collected at a temporal resolution of once every six days, with a 24-hour sampling period (10:00 a.m. to 10:00 a.m. the next day) for PAMS and a 3-hour sampling period (12:00 p.m. to 3:00 p.m.) for OVOCs. The PAMS and OVOC components were analyzed by gas chromatography–mass spectrometry (Model Trace-DSQ II, Thermo Fisher) and liquid chromatography (Model 1260, Agilent Technologies Inc.), respectively. Detailed chemical analysis and quality control of $PM_{2.5}$ and volatile organic compounds (VOCs) for Linyi were obtained from our previous study (Liu et al., 2025b; Wang et al., 2023) (see Texts S1&S2 in Supplementary material).

2.4 RF model

This study implemented the RF model (Python 3.11.9) to quantitatively assess the relative contributions of anthropogenic emissions and meteorological factors to $PM_{2.5}$ and O_3 pollution. The model incorporated temporal indicators and meteorological factors as predictive variables. Temporal indicators, including Unix time (number of seconds since January 1, 1970), day of year, day of week, and hour of day, served as proxies for anthropogenic emissions at different time scales. Specifically, Unix time captured long-term trends influenced by industrialization and policy interventions, while day of year represented seasonal variations in emissions and atmospheric chemistry. Day of week reflected weekly emission cycles, and hour of day captured diurnal patterns, particularly NO_x fluctuations associated with traffic activity (Grange et al., 2018; Liu et al., 2022; Shi et al., 2021; Song et al., 2023). It is important to note that temporal variables are indirect proxies for anthropogenic emissions rather than direct measurements. This approach assumes that periodic temporal patterns reflect periodic emission patterns from human activities, which is a common practice in meteorological normalization studies. However, attribution results derived from such proxy variables should be interpreted with caution. Independent validation using high-resolution dynamic emission inventories is needed to further confirm the robustness of these findings. Meteorological factors encompassed WS, RH, T, SP, TP, BLH, SSRD, TCC and atmospheric oxidizing potential. Among these, we used total oxidant O_x ($O_x = O_3 + NO_2$) to characterize the atmospheric oxidizing potential (Dai et al., 2022). For model development, monitoring data from identical periods in 2022 and 2023 were integrated and partitioned into training (80%) and testing (20%) subsets. This data splitting strategy facilitated robust model performance evaluation through standard ML validation protocols (Fig. 1). To assess potential overfitting, we compared model performance on the training and test sets. If the difference in coefficients of determination (R^2) values between the training set and the test set is less than 5%, this indicates a low risk of overfitting.

Given the significant impact of interannual variations in meteorological factors on pollutant concentrations, this study implemented rigorous meteorological normalization to eliminate the interference of meteorological variability (Grange et al., 2018; Grange & Carslaw, 2019). Specifically, for a specific time point, we randomly sampled

combinations of meteorological variables from the integrated data, input them into the trained model along with the corresponding time variables for prediction, repeated this process 1,000 times, and took the average to obtain the meteorologically normalized concentration (referred to as the "de-weathered concentration") for that time point. This concentration metric excludes the influence of meteorological factors and purely reflects anthropogenic emission characteristics. For O_3 pollution assessment, we further calculated the de-weathered MDA8-O_3 based on the de-weathered O_3 concentration. We use the following equation to assess the impact of anthropogenic emissions and meteorological factors on changes in pollutant concentrations.

$$E = \frac{C^{p}_{2023} - C^{p}_{2022}}{C^{ob}_{2022}} \times 100\% \quad (1)$$

$$M = \frac{(C^{p}_{2022} - C^{p}_{2023}) - (C^{ob}_{2022} - C^{ob}_{2023})}{C^{ob}_{2022}} \times 100\% \quad (2)$$

where E and M represent the contributions of anthropogenic emissions and meteorological factors (%) to changes in pollutant concentrations, respectively. C^{ob}_{2023} and C^{p}_{2023} represent the observed and de-weathered concentrations (μg/m^3) in 2023, respectively. C^{ob}_{2022} and C^{p}_{2022} represent the observed and de-weathered concentrations in 2022, respectively.

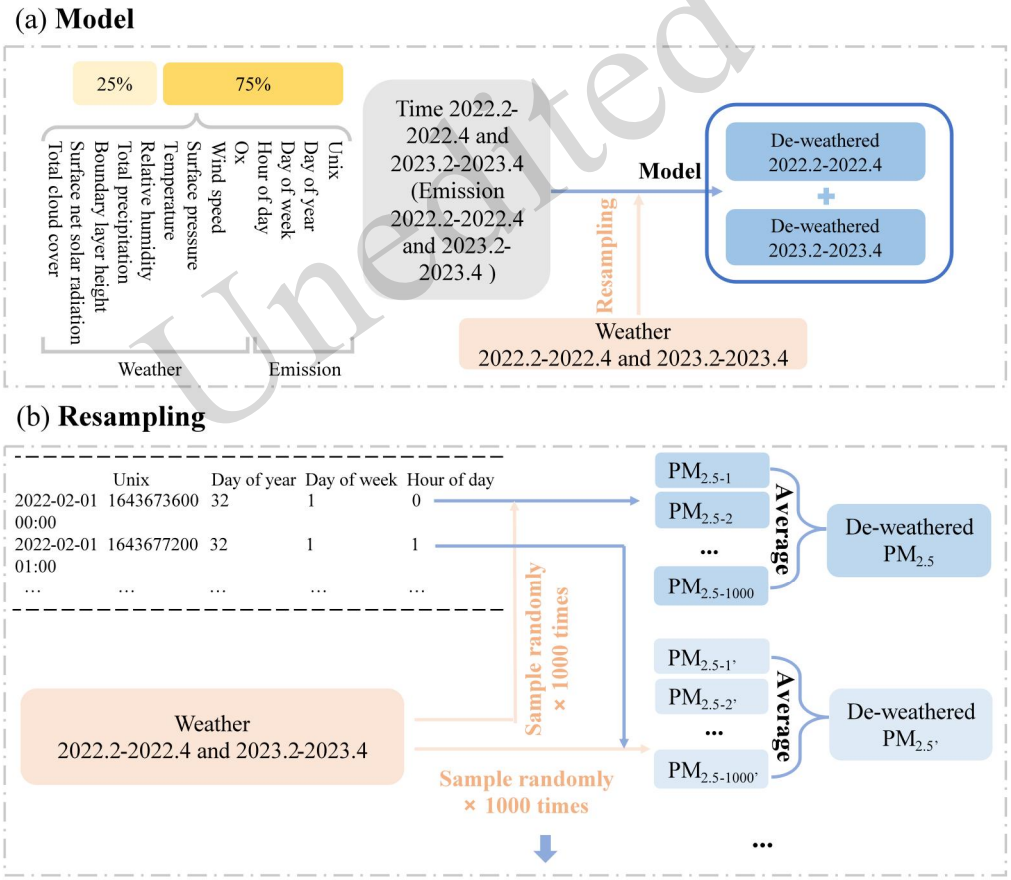

Fig. 1. (a) The establishment of random forest regression models and (b) the resampling process of the de-weather method (taking the early spring period of $PM_{2.5}$ as an example).

2.5 SHAP algorithm

The SHAP algorithm, grounded in cooperative game theory, quantifies the marginal contribution of each feature to model predictions through Shapley values (Li et al., 2024; Lundberg et al., 2020). For a random forest model with p features, the SHAP value for feature j in a given prediction is defined as (Esu et al., 2024; Hossain & Roy, 2025):

$$\mathrm{SHAP}(X_j) = \sum_{S \in N} \frac{k!(p-k-1)!}{p!} [f(S \cup \{j\}) - f(S)] \quad (3)$$

where p is the total number of features, N is a set of all possible combinations of features excluding X_j, S is a feature set in N, $f(S)$ is the model prediction with features in S, and $f(S\cup\{j\})$ is the model prediction with features in S plus feature X_j. SHAP values satisfy three desirable properties: efficiency (contributions sum to the difference between prediction and baseline), symmetry (equal marginal effects receive equal attribution), and additivity (consistent attribution across model ensembles).

This framework provides a theoretically consistent interpretation of individual predictions, making it particularly suitable for identifying the direction and magnitude of each feature's influence on $PM_{2.5}$ and O_3 concentrations.

3 Results and discussion

3.1 Variations in $PM_{2.5}$ and O_3 in 2022–2023

In 2023, Shandong Province experienced notable increases in both $PM_{2.5}$ and O_3 concentrations compared with 2022 (Fig. 2). The annual average $PM_{2.5}$ concentration reached 39.2±28.9 μg/m^3, exceeding China's national secondary standard (35.0 μg/m^3) by 12% and representing a 7.1% increase over the 2022 level (36.6±23.4 μg/m^3). To identify periods with the most pronounced $PM_{2.5}$ increases, we first compared monthly average concentrations between the two years. Based on this comparison, two periods showed consistently higher $PM_{2.5}$ levels in 2023: the early spring period (ESP, February to April) and the autumn harvest period (AHP, September to October). During the ESP, the average $PM_{2.5}$ concentration was 48.5±25.8 μg/m^3—19.8% higher than that in the same period of 2022 (40.5±16.4 μg/m^3)—along with 13 more exceedance days. During the AHP, average $PM_{2.5}$ concentrations reached 32.9±16.4 μg/m^3, a 20.1% increase over 2022 (27.4±15.5 μg/m^3), with October alone exhibiting a 24.7% monthly increase. To gain deeper insight into the drivers of $PM_{2.5}$ rebound, we analyzed its chemical composition during the two key periods (Fig. 3). Concentrations of major secondary inorganic aerosols (SIA, including SO_4^{2-}, NO_3^-, and NH_4^+) and OM showed increasing trends during both the ESP and AHP of 2023 compared with 2022. During the ESP, NO_3^-, the dominant SIA component, increased by 11.6%, while SO_4^{2-} and NH_4^+ rose by 6.9% and 10.9%, respectively. Similarly, during AHP, SO_4^{2-} and NO_3^- showed increases of 22.2% and 13.4%, respectively. The concurrent increasing trends in SIA and OM suggest possible enhanced secondary aerosol formation in 2023, potentially driven by intensified anthropogenic emissions and meteorological conditions conducive to atmospheric chemical reactions.

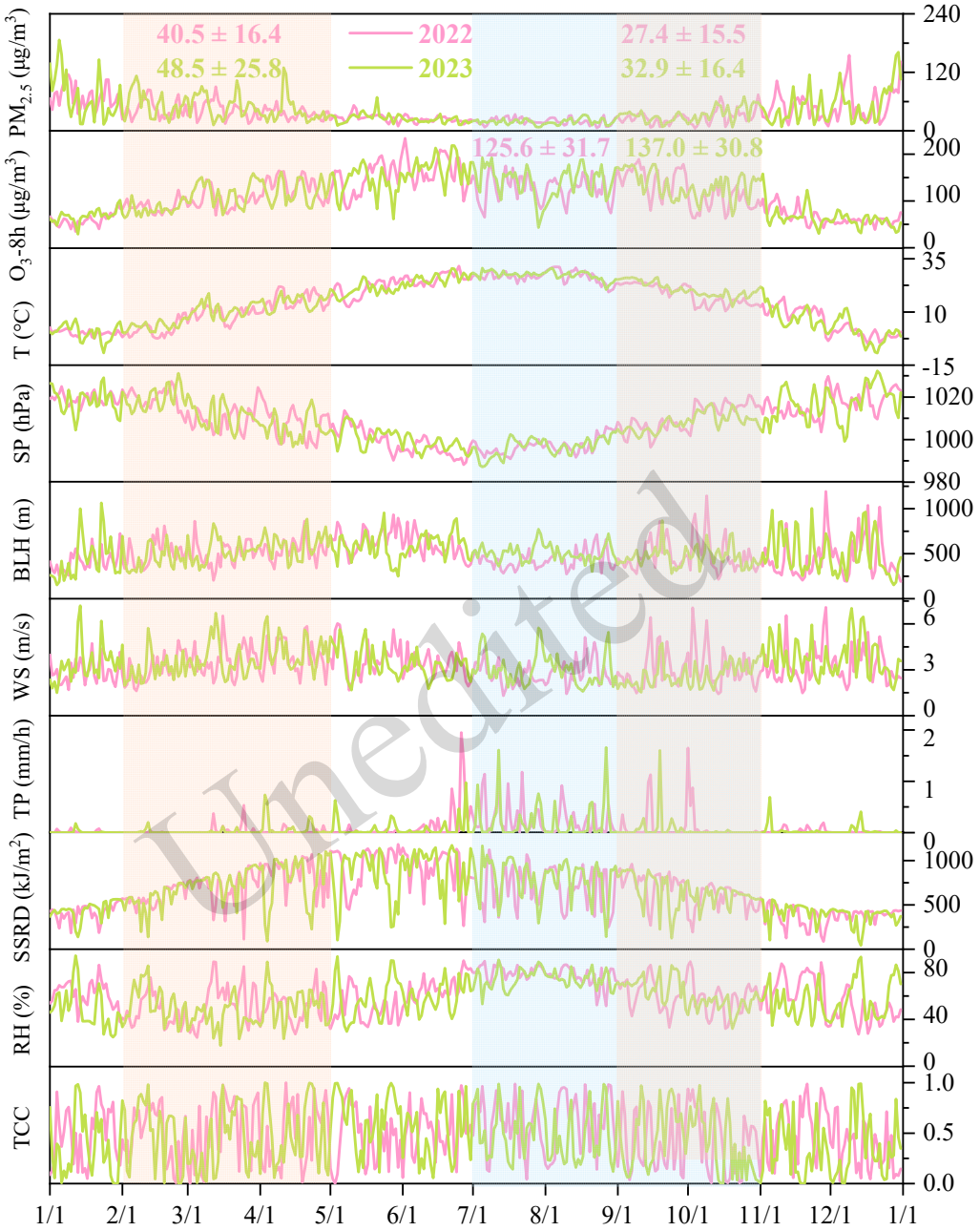

Fig. 2. Time series of air pollutant concentrations and meteorological factors in Shandong Province from 2022 to 2023. The shaded regions represent three distinct pollution periods, the early spring period (ESP, February to April), the photochemical season period (PSP, July to October), and the autumn harvest period (AHP, September to October) from left to right.

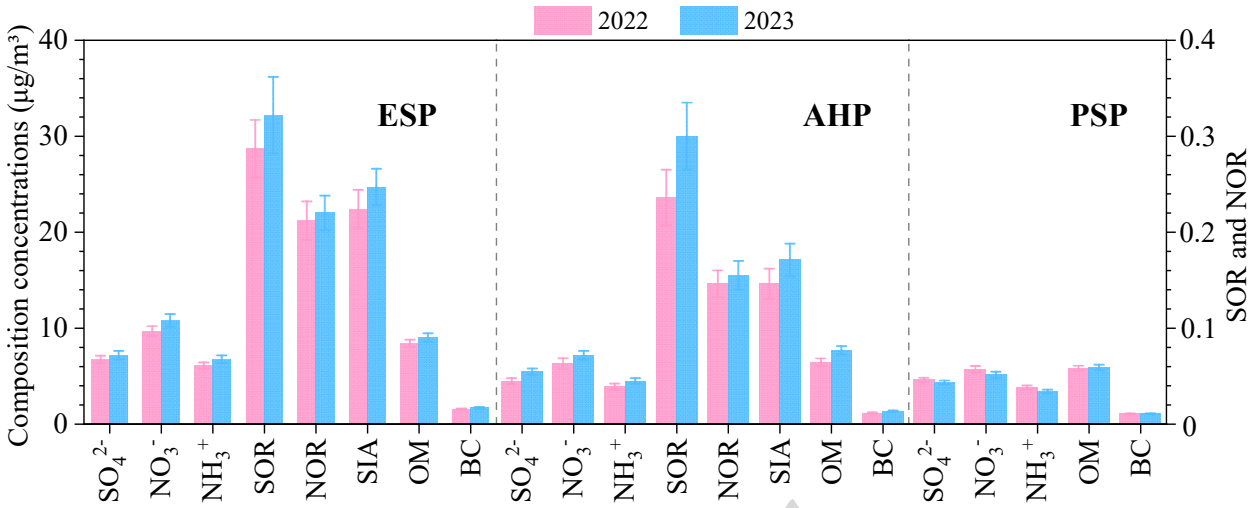

Fig. 3. Chemical composition across different pollution periods in Shandong Province. All differences between 2022 and 2023 are not statistically significant (Mann–Whitney U test, $p > 0.05$). SOR: sulfur oxidation ratio. NOR: nitrogen oxidation ratio. Detailed calculations of SOR and NOR are provided in Text S3.

Meanwhile, the 90th-percentile maximum daily 8-hour average O_3 concentration (MDA8-O_3-90%) increased from 167.9 μg/m^3 in 2022 to 171.8 μg/m^3 in 2023. O_3 pollution was particularly severe from July to October (photochemical season period, PSP), with a 9.1% year-on-year increase and 12 additional exceedance days. These pollution rebounds show strong correlations with both anthropogenic emissions and meteorological factors, underscoring the need for quantitative assessment of their relative contributions.

3.2 Model performance optimization and evaluation

The performance of random forest models is highly sensitive to parameter configuration. Conventional approaches often rely on default parameter settings (e.g., n_estimators = 300, max_depth = 3, max_features = 3), which may fail to accommodate the distinct characteristics of different pollution periods, potentially resulting in suboptimal model performance. To overcome this limitation, we adopted the TPE sampler within the Optuna framework for hyperparameter optimization (Lee et al., 2025). Through 300 iterations of guided search, we identified optimal parameter configurations for each pollution period: ESP with n_estimators = 130, max_depth = 15, max_features = 6; AHP with n_estimators = 332, max_depth = 15, max_features = 6; and PSP with n_estimators = 358, max_depth = 15, max_features = 5 (Tables S1–S3). To ensure the robustness of the optimization results, we further performed cross-validation using five randomly selected parameter combinations. The TPE-optimized configurations consistently delivered superior model performance, confirming the reliability of the Bayesian optimization approach. The small difference between training and test R^2 (< 5%) indicated a low risk of overfitting, suggesting that the model predictions and the resulting SHAP attributions are robust within the tested hyperparameter space. This adaptive parameter-tuning strategy not only improves the characterization of nonlinear relationships between gaseous pollutants and their drivers but also enhances period-specific modeling capabilities, thereby providing a solid methodological foundation for accurately quantifying contributions from anthropogenic emissions and meteorological factors.

The random forest models developed for the three pollution periods exhibited excellent predictive performance (Fig. 4). For the ESP, the model achieved an R^2 of 0.95 on the test set, with root mean square error (RMSE) and mean absolute error (MAE) values of 5.29 μg/m^3 and 2.84 μg/m^3, respectively, indicating a strong capability to capture early spring pollution dynamics. The AHP model also performed exceptionally well, yielding an R^2 of 0.96 on the test set with low prediction errors (RMSE = 3.24 μg/m^3; MAE = 2.11 μg/m^3). The PSP model maintained a high test-set R^2 value of 0.94, demonstrating robust

performance in simulating complex photochemical processes. The R^2 values for the training sets of all three models were 0.99. Importantly, the test set R^2 values remained high (0.94–0.96), with a difference of less than 5% between training and test performance. This small gap demonstrates strong generalization capability and a low risk of overfitting, despite the high training R^2.

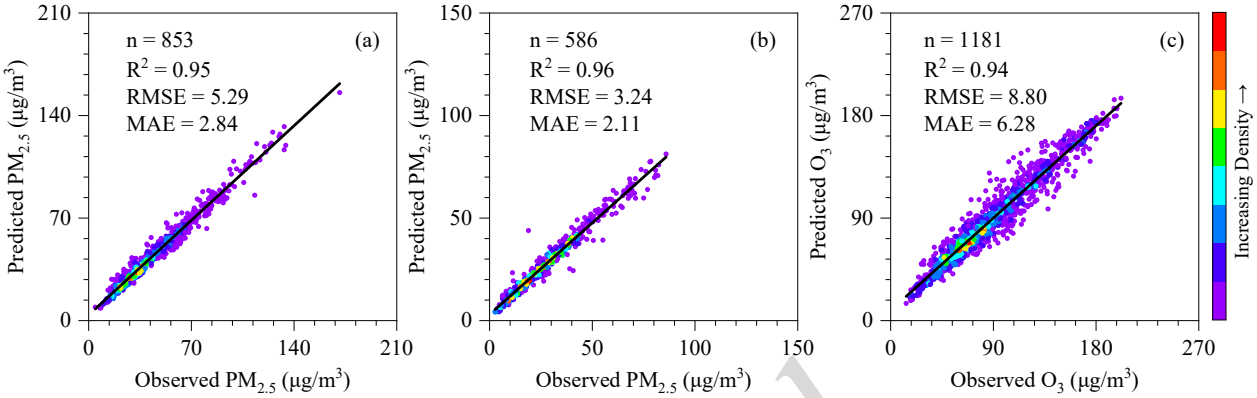

Fig. 4. Performance of RF models on $PM_{2.5}$ or O_3 concentrations during (a) ESP, (b) AHP, and (c) PSP. *n*: number of data points. The units of RMSE and MAE are $\mu g/m^3$.

3.3 Impacts of emissions and meteorology on $PM_{2.5}$ rebound

Through SHAP value analysis, we systematically quantified the relative contributions of anthropogenic emissions and meteorological factors to $PM_{2.5}$ formation. The SHAP values—indicating both the magnitude and direction of feature impacts—showed that temporal variables (Unix time and day of year) exerted the strongest influence during both the ESP and AHP (Figs. 5a and b). These temporal patterns primarily reflect long-term anthropogenic emission trends. Although anthropogenic emissions were the dominant driver of pollution rebound, meteorological factors during the ESP still played a notable role (Tables S4 and S5).

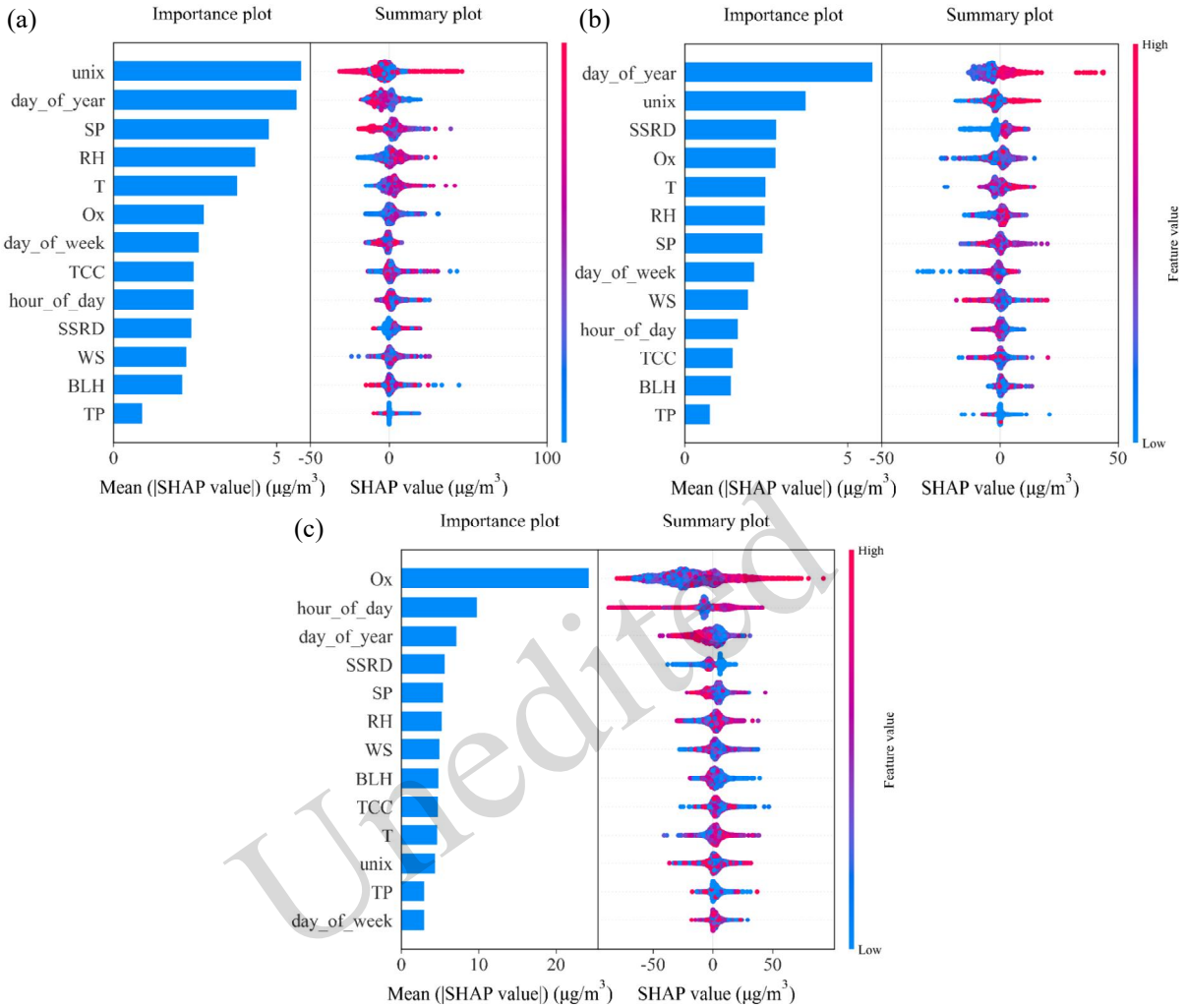

Fig. 5. Feature importance results of the RF-SHAP model during (a) ESP, (b) AHP, and (c) PSP. Left: mean absolute SHAP values. Right: SHAP value analysis of factors influencing $PM_{2.5}$ or O_3 formation. Positive SHAP values indicate variables that enhance $PM_{2.5}$ or O_3 concentration, while negative values reflect those that reduce concentration levels. Notably, data points in pink exhibit greater influence due to their higher feature values.

Quantitatively, anthropogenic emissions accounted for 14.1% of the $PM_{2.5}$ increase during the ESP, substantially exceeding the contribution from meteorological factors (5.7%; Fig. 6a). Song et al. (2025) studied a severe $PM_{2.5}$ rebound event in February 2023 over the North China Plain and reported relative contributions of 48.1% (anthropogenic) and 33.4% (meteorological). Although both studies identify anthropogenic emissions as the dominant driver, the magnitudes differ considerably. This discrepancy likely reflects differences in the study period (multimonth and single episode), spatial scale (Shandong and North China Plain), and methodological approaches (RF-SHAP and other methods). Such comparisons highlight the importance of context-specific factors in pollution rebound analyses. The contrast was even more pronounced during the AHP, where anthropogenic emissions contributed 19.0%, compared with only 1.1% from meteorological factors (Fig. 6b). These results indicate that the relative influence of anthropogenic emissions and meteorological conditions on $PM_{2.5}$ varies considerably across different seasons. Based on a high-resolution emission inventory analysis, this study quantifies changes in pollutant emissions during the ESP period in 2023 relative to the same period in 2022. The results indicate substantial increases in total $PM_{2.5}$ and PM_{10} emissions, both rising by 16.4%. Emissions of NO_x and VOCs—key precursors of secondary

particulate matter—also increased by 16.5% and 19.8%, respectively (Fig. 7a). This concurrent rise suggests a potential intensification of secondary pollution formation. To further identify the drivers behind these increases, we analyzed sector-specific contribution ratios. The industrial sector emerged as the dominant contributor, accounting for 70.4%, 56.0%, and 68.2% of the increases in $PM_{2.5}$, NO_x, and VOC emissions, respectively (Fig. 7b). These findings form a coherent and mutually reinforcing evidence chain alongside macroscale observations. On the one hand, they are consistent with the recovery in industrial activity, as reflected by the 9.2% year-on-year increase in industrial energy consumption in Shandong Province (Fig. S1). On the other hand, they directly explain the 19.5% year-on-year surge in NO_2 concentrations observed during the ESP period in environmental monitoring data (Table 1). The pronounced increase in industrial emissions produced strong compound pollution effects. The substantial release of NO_x and VOC precursors enhanced the formation of secondary nitrates and secondary organic aerosols (SOA) through accelerated atmospheric photochemical processes. Overall, this study not only quantifies the dominant role of industrial sources in primary pollutant emissions but also reveals their critical contribution to regional composite pollution formation, offering key insights into the drivers of atmospheric pollution in the postpandemic era. The transportation sector also played a notable role in the emission increase. Based on the same emission inventory, the transportation sector contributed 23.7% of NO_x and 21.8% of VOCs in the total emission increments during the ESP period. These source apportionment results are consistent with macrolevel statistics: in 2023, passenger traffic in Shandong Province increased by 100.2% and highway freight turnover by 65.3% compared to 2022. Therefore, strengthening pollution control in the transportation sector is of critical importance for mitigating secondary pollution. Moreover, satellite observations revealed a 70.0% increase in crop residue burning incidents during the 2023 AHP (http://satsee.radi.ac.cn:8080/index.html), emitting large quantities of $PM_{2.5}$ precursors and primary organic carbon (POC). Chemical composition analyses of $PM_{2.5}$ in Linyi further corroborated these findings. Compared with 2022, the annual growth rate of POC in Linyi reached 62.4% (Fig. 8), significantly exacerbating $PM_{2.5}$ pollution levels.

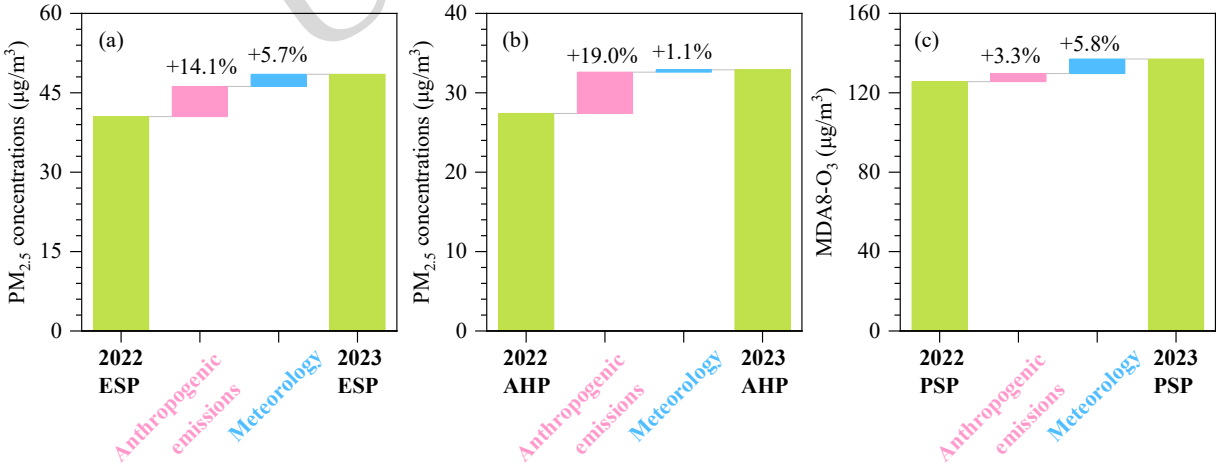

Fig. 6. Contributions of anthropogenic emissions and meteorological factors to $PM_{2.5}$ or O_3 pollution during (a) ESP, (b) AHP, and (c) PSP.

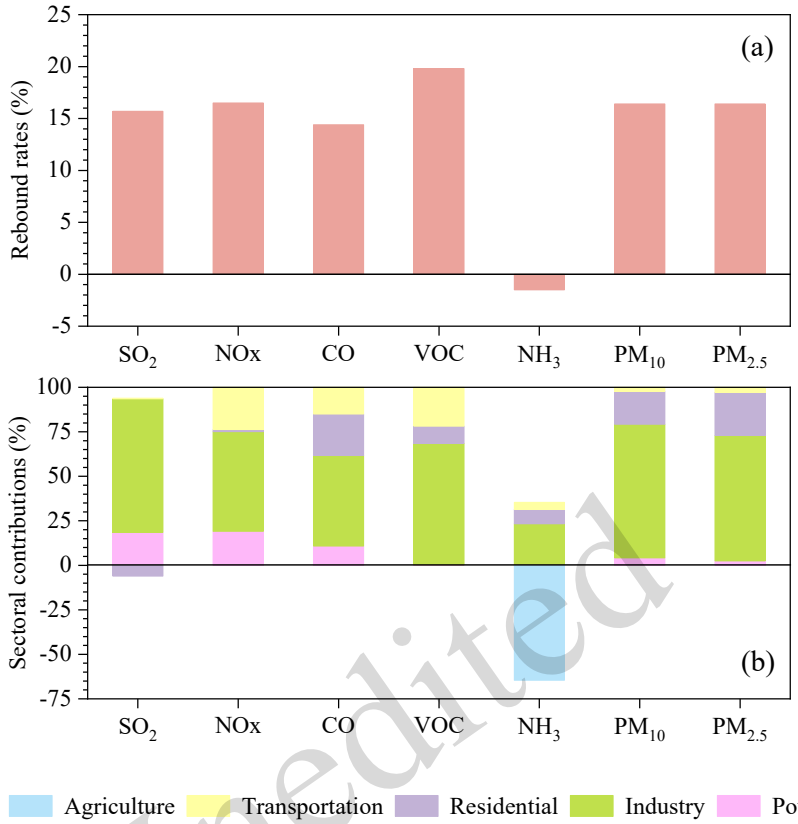

Fig. 7. (a) Emission rebound rate and (b) sectoral contribution to the emission rebound for SO_2, NO_x, CO, VOC, NH_3, PM_{10}, and $PM_{2.5}$ during 2023 ESP compared to 2022 ESP. The emission inventory in Shandong Province was obtained from the Multiresolution Emission Inventory for China (MEIC, http://meicmodel.org.cn).

Table 1. Statistical summary of air pollutant concentrations and meteorological factors during different periods (mean±standard deviation)

Periods	SO_2 ($\mu g/m^3$)	NO_2 ($\mu g/m^3$)	T (°C)	SP (hPa)	BLH (m)	WS (m/s)	TCC	SSRD (kJ/m^2)	RH (%)	TP (mm/h)	O_x ($\mu g/m^3$)
2022	11.1	25.1	8.9	1011.8	516.9	3.52	0.51	717.0	50.8	2.4E-02	104.7±26.2
ESP	± 2.2	± 7.4	± 6.0	± 7.5	± 132.4	± 1.02	± 0.29	± 217.0	± 14.7	± 6.0E-02	
2023	10.8	30.0	9.9	1011.9	525.6	3.66	0.44	709.1	49.2	3.4E-02	107.2±27.4
ESP	± 3.7	± 12.2	± 6.4	± 7.8	± 175.1	± 1.12	± 0.31	± 230.5	± 15.4	± 9.6E-02	
2022	10.2	28.5	18.2	1010.2	489.3	3.07	0.40	655.8	59.7	9.8E-02	109.7±36.7
AHP	± 2.0	± 9.0	± 4.5	± 6.3	± 183.4	± 1.26	± 0.29	± 173.2	± 13.5	± 3.0E-01	
2023	9.2	29.8	20.7	1008.1	465.8	2.61	0.44	637.7	60.8	5.1E-02	118.6±34.7
AHP	± 1.7	± 8.9	± 3.3	± 4.3	± 109.7	± 0.74	± 0.30	± 171.2	± 12.0	± 2.0E-01	
2022	8.9	21.8	22.5	1003.5	460.2	2.92	0.51	679.9	69.2	1.7E-01	108.3±34.8
PSP	± 2.0	± 9.5	± 5.6	± 8.5	± 149.0	± 1.06	± 0.30	± 200.3	± 14.4	± 3.1E-01	
2023	8.1	23.2	24.1	1002.3	487.5	2.82	0.47	718.6	67.7	1.2E-01	117.4±37.4
PSP	± 1.8	± 10.2	± 4.3	± 7.1	± 102.0	± 0.92	± 0.28	± 210.2	± 12.2	± 2.9E-01	

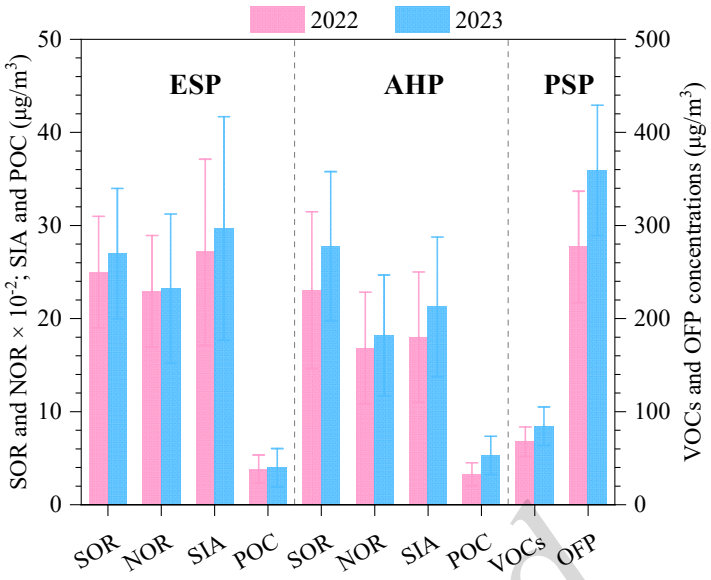

Fig. 8. Multiparameter analysis of air pollution in a typical city in Shandong Province during ESP, AHP, and PSP. OFP: ozone formation potential. A detailed calculation of OFP is provided in Text S3.

Concurrently, meteorological analyses identified temperature increases as a key environmental factor, with recorded rises of 1.0 °C and 2.5 °C during the ESP and AHP, respectively (Table 1). Notably, SHAP feature dependence plots showed that higher temperatures consistently corresponded to more positive SHAP values, indicating that temperature exerted a strong positive effect on pollutant formation (Figs. 9a and 9b). Higher temperatures enhance the positive contribution of O_x and industrial emissions to $PM_{2.5}$. Mechanistically, the elevated temperature accelerated the liquid-phase oxidation of SO_2, shifted NH_4NO_3 thermal decomposition toward the gaseous phase, and enhanced VOC reactivity, collectively promoting secondary aerosol formation (Liu et al., 2025a; Xu et al., 2019). This warming directly enhanced atmospheric oxidation capacity, as evidenced by the increased SOR and NOR across Shandong Province. In 2023, both SOR and NOR increased compared to 2022, particularly during the AHP, where SOR rose from 0.23 to 0.30 and NOR from 0.15 to 0.16. Consequently, the total concentration of SIAs increased by 10.0% (ESP) and 16.6% (AHP) province-wide (Fig. 3). This province-wide trend was prominently reflected in Linyi, a typical industrial city. Compared with 2022, the SOR during the ESP and AHP periods in Linyi increased by 8.0% and 20.6%, respectively, in 2023, while the NOR also showed an upward trend. Against this backdrop, the concentrations of SIA increased concurrently by 9.4% and 18.1% (Fig. 8).

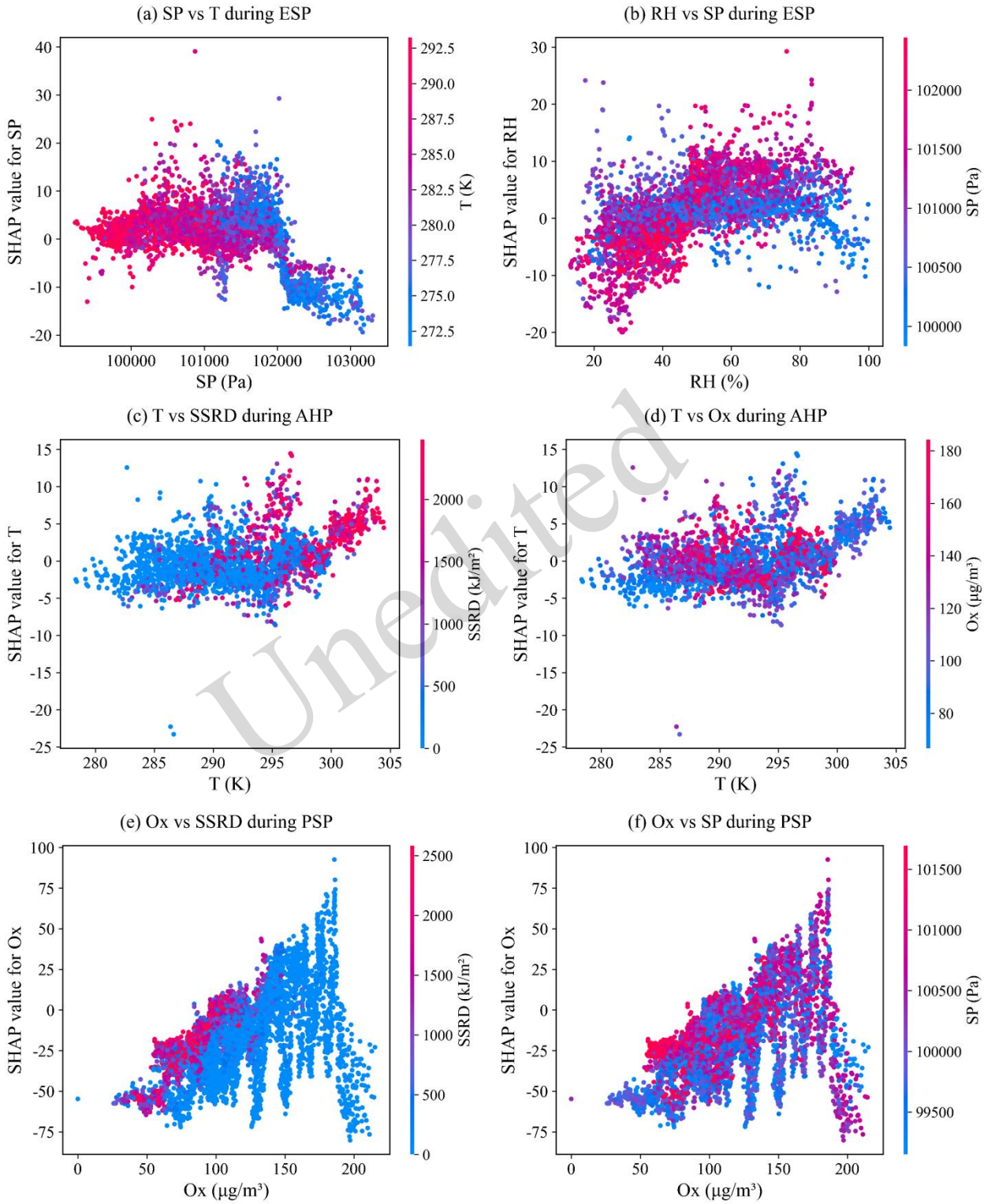

Fig. 9. SHAP feature dependence plots.

3.4 Impacts of emissions and meteorology on O_3 rebound

Compared with $PM_{2.5}$, O_3 concentration variability during the PSP exhibited distinct driving characteristics, with its rebound primarily governed by enhanced atmospheric oxidizing capacity. Quantitative analysis showed that meteorological

factors contributed substantially more to the O_3 increase (5.8%) than anthropogenic emissions (3.3%) (Fig. 6c). This disparity was mainly attributed to intensified atmospheric chemical processes induced by the unique meteorological anomalies of 2023. Observational data indicated that, relative to 2022, total cloud cover in Shandong Province decreased by 7.8% (from 0.51±0.30 to 0.47±0.28), directly strengthening net surface radiation (from 679.9±200.3 to 718.6±210.2 kJ/m²) (Table 1). This radiation-driven change in the photochemical environment markedly enhanced the atmospheric oxidation capacity, as reflected by the increase in total oxidant (O_x) from 108.3±34.8 μg/m^3 in the 2022 PSP to 117.4±37.4 μg/m^3 in the 2023 PSP. More importantly, SHAP interaction analysis showed that elevated O_x consistently corresponded to higher positive SHAP values (Figs. 9e and 9f), confirming the central role of the oxidizing potential in driving O_3 formation from the perspective of model interpretability. Enhanced radiation accelerated photochemical reaction rates—particularly NO_2 photolysis—thereby promoting O_3 production (Yao et al., 2025a; Zhang et al., 2025b). Additionally, an increase in boundary layer height (BLH, from 460.2±149.0 to 487.5±102.0 m) facilitated vertical mixing, reduced near-surface NO concentrations, and weakened O_3 depletion through NO titration (Liu & Wang, 2020). These combined effects ultimately led to enhanced surface O_3 accumulation. This meteorologically driven O_3 enhancement is consistent with findings from the South Coast Air Basin, where heatwaves and stagnant conditions have been shown to promote O_3 production and accumulation (Wu et al., 2023).

Regarding anthropogenic influences, the rapid rebound of socioeconomic activity following the relaxation of COVID-19 restrictions significantly increased emissions of O_3 precursors. In 2023, Shandong Province experienced a 103% surge in passenger traffic compared with 2022 (rising from 163.7 million to 332.6 million person-times), while highway freight turnover grew by 65.3% (from 9.8 billion to 16.2 billion passenger-km) (Fig. S1). This resurgence in transportation contributed to a 6.4% increase in vehicular NO_2 emissions (Table 1). Furthermore, the expansion of the petrochemical sector intensified O_3 formation. Statistical data show that the number of enterprises in five major petrochemical-related sectors—including petroleum and coal processing and chemical product manufacturing—increased from 5,352 to 5,904 (a 10.3% rise) in 2023 (Fig. S1). These industrial activities substantially increased VOC emissions. For instance, in Linyi, the average daily VOC concentration during the 2023 PSP reached 84.3 μg/m^3, compared with 67.5 μg/m^3 in 2022. The increase in precursor emissions directly resulted in a significant rise in OFP. During the 2023 PSP, the average daily OFP increased by 29.7% relative to that in 2022, underscoring Linyi's representative role in illustrating the province-wide trend of worsening O_3 pollution (Fig. 8).

4 Conclusions

This study employed random forest modeling combined with SHAP analysis to identify the key drivers behind the $PM_{2.5}$ and O_3 pollution rebounds observed in Shandong Province in 2023. The results show that $PM_{2.5}$ increases were primarily driven by anthropogenic emissions (14.1% during ESP; 19.0% during AHP), particularly from industrial activities and agricultural residue burning. Meteorological conditions—especially elevated temperatures—further amplified secondary aerosol formation through enhanced atmospheric chemical processes. In contrast, O_3 pollution exhibited a stronger dependence on meteorological influences (5.8% during PSP), although precursor emissions from the transportation and petrochemical industries remained indispensable for O_3 production.

These findings underscore the need for seasonally differentiated control strategies: industrial and agricultural emission reductions should be prioritized in spring and autumn to mitigate $PM_{2.5}$ pollution, whereas summer policies should emphasize meteorological monitoring in conjunction with precursor emission control to curb O_3 formation. This study provides important scientific support for reconciling economic recovery with air quality improvement in Shandong Province during the postpandemic period. Future research should incorporate dynamic emission inventories and enhanced meteorological observations to further improve pollution forecasting and management

systems.

We acknowledge that our sectoral analysis focused primarily on industry, agriculture, and transportation, while the residential combustion and power generation sectors were not examined in detail. Based on preliminary inventory analysis, these two sectors showed relatively small year-on-year emission changes in 2023 compared to the sectors analyzed and thus were not the main drivers of the pollution rebound. Nevertheless, future work with higher-resolution emission inventories should include a more comprehensive sectoral breakdown covering residential and power sources to further validate the findings. Another limitation of this study is that we did not explicitly quantify the contribution of long-range transport or regional pollutant inflow to the PM2.5 rebound. Future research should integrate chemical transport models or receptor-based methods to better resolve transboundary influences.

Acknowledgments

This work was supported by the National Science Foundation of China [Grant No. 42507143] and the Shandong Postdoctoral Science Foundation [Grant No. SDCX-ZG-202303008].

Author contributions

Gang Wang: Formal analysis, Investigation, Methodology, Writing – original draft. **Sai Liu:** Data curation, Investigation, Methodology, Software, Validation, Writing – original draft. **Kai Wang & Huijuan Meng & Hanyu Zhang:** Writing – review & editing. **Na Zhao:** Methodology, Funding acquisition, Writing – review & editing.

Conflict of interest

The authors declare that there are no conflicts of interest or personal relationships that could have appeared to influence the work reported in this paper.

Data availability

The data that support the findings of this study are available from the corresponding author upon reasonable request.

References

Assareh N, Beddows A, Stewart G, et al., 2025. What impact does net zero action on road transport and building heating have on exposure to UK air pollution? *Environ. Sci. Technol.*, 59, 1274–1286. https://doi.org/10.1021/acs.est.4c05601.

Belis CA, Pernigotti D, Pirovano G, et al., 2020. Evaluation of receptor and chemical transport models for PM_{10} source apportionment. *Atmos. Environ. X.*, 5, 100053. https://doi.org/10.1016/j.aeaoa.2019.100053.

Chen Y, Zhu L, Wang S, et al., 2025. Unraveling the complexities of ozone and $PM_{2.5}$ pollution in the Pearl River Delta region: Impacts of precursors emissions and meteorological factors, and effective mitigation strategies. *Atmos. Pollut. Res.*, 16, 102368. https://doi.org/10.1016/j.apr.2024.102368.

Dai S, Chen X, Liang J, et al., 2023. Response of $PM_{2.5}$ pollution to meteorological and anthropogenic emissions changes during COVID-19 lockdown in Hunan Province based on WRF-Chem model. *Environ. Pollut.*, 331, 121886. https://doi.org/10.1016/j.envpol.2023.121886.

Dai Y, Cai X, Zhong J, et al., 2022. Chemistry, transport, emission, and shading effects on NO_2 and O_x distributions within urban canyons. *Environ. Pollut.*, 315, 120347. https://doi.org/10.1016/j.envpol.2022.120347.

Elbir T, Tuygun GT, Gundogdu S, et al., 2025. Evaluating Machine Learning-Based $PM_{2.5}$ Estimation Using Integrated High-Resolution Datasets Across NDVI Levels in an Urban-Industrialized Region. *Environ. Pollut.*, 126734. https://doi.org/10.1016/j.envpol.2025.126734.

Esu CO, Pyo J, Cho K, 2024. Machine learning-derived dose-response relationships considering interactions in mixtures: Applications to the oxidative potential of particulate matter. *J. Hazard. Mater.*, 134864. https://doi.org/10.1016/j.jhazmat.2024.134864.

Grange SK, Carslaw DC, 2019. Using meteorological normalisation to detect interventions in air quality time series. *Sci. Total Environ.*, 653, 578–588. https://doi.org/10.1016/j.scitotenv.2018.10.344.

Grange SK, Carslaw DC, Lewis AC, et al., 2018. Random forest meteorological normalisation models for Swiss PM_{10} trend analysis. *Atmos. Chem. Phys.*, 18, 6223–6239. https://doi.org/10.5194/acp-18-6223-2018.

Hossain MM, Roy K, 2025. The development of classification-based machine-learning models for the toxicity assessment of chemicals associated with plastic packaging. *J. Hazard. Mater.*, 136702. https://doi.org/10.1016/j.jhazmat.2024.136702.

Hou L, Dai Q, Song C, et al., 2022. Revealing drivers of haze pollution by explainable machine learning. Environ. *Sci. Technol. Lett.*, 9, 112–119. https://doi.org/10.1021/acs.estlett.1c00865.

Hou X, Wang X, Cheng S, et al., 2025. Evaluating urban carbon neutrality pathways and co-benefits through an integrated downscaling framework: A case study of the Beijing–Tianjin–Hebei region, China. *Environ. Sci. Technol.* https://doi.org/10.1021/acs.est.5c12973.

Jia H, Yao S, Tang X, et al., 2026. Multi-objective machine learning for health-oriented O_3 and $PM_{2.5}$ control: Integrating VOC photochemical consumption and source apportionment. *J. Hazard. Mater.*, 505, 141483. https://doi.org/10.1016/j.jhazmat.2026.141483.

Jiang F, Ma J, 2025. Graph-based machine learning for

high-resolution assessment of pedestrian-weighted exposure to air pollution. Resour. *Environ. Sustainability*, 20, 100219. https://doi.org/10.1016/j.resenv.2025.100219.

Kim HK, Kim E, Song CK, et al., 2025. Comparative evaluation of surface-level $PM_{2.5}$ modeling across Northeast Asia: relevance for regulatory and scientific applications. *Environ. Pollut.*, 126428. https://doi.org/10.1016/j.envpol.2025.126428.

Lee BG, Jeong KH, Kim HE, et al., 2025. Machine learning models for predicting indoor airborne fungal concentrations in public facilities utilizing environmental variables. *Environ. Pollut.*, 368, 125684. https://doi.org/10.1016/j.envpol.2025.125684.

Levi Y, Broday DM, 2024. Revealing causality in the associations between meteorological variables and air pollutant concentrations. *Environ. Pollut.*, 123526. https://doi.org/10.1016/j.envpol.2024.123526.

Li J, Liu X, Wang H, et al., 2024. Prediction and interpretation of photocatalytic NO removal on g-C_3N_4-based catalysts using machine learning. *Chin. Chem. Lett.*, 35, 108596. https://doi.org/10.1016/j.cclet.2023.108596.

Li K, Jacob DJ, Liao H, et al., 2019. A two-pollutant strategy for improving ozone and particulate air quality in China. *Nat. Geosci.*, 12, 906–910. https://doi.org/10.1038/s41561-019-0464-x.

Li K, Sun R, 2024. Understanding the driving mechanisms of site contamination in China through a data-driven approach. *Environ. Pollut.*, 342, 123105. https://doi.org/10.1016/j.envpol.2023.123105.

Li S, Wang S, Wu Q, et al., 2023. Emission trends of air pollutants and CO_2 in China from 2005 to 2021. *Earth Syst. Sci. Data.*, 15, 2279–2294, https://doi.org/10.5194/essd-15-2279-2023.

Liu H, Yue F, Xie Z, 2022. Quantify the role of anthropogenic emission and meteorology on air pollution using machine learning approach: A case study of $PM_{2.5}$ during the COVID-19 outbreak in Hubei Province, China. *Environ. Pollut.*, 300, 118932. https://doi.org/10.1016/j.envpol.2022.118932.

Liu S, Wang G, Kong F, et al., 2025a. Chemical composition, multiple sources, and health risks of $PM_{2.5}$: A case study in Linyi, China's plate and logistics capital. *Environ. Pollut.*, 365, 125343. https://doi.org/10.1016/j.envpol.2024.125343.

Liu S, Wang G, Kong F, et al., 2025b. $PM_{2.5}$ pollution characteristics, drivers, and regional transport during different pollution levels in Linyi, China: An integrated PMF-ML-SHAP framework and transport models. *J. Hazard. Mater.*, 494, 138534. https://doi.org/10.1016/j.jhazmat.2025.138534.

Liu S, Wang G, Zhao N, et al., 2025c. Ozone pollution in a typical region of southeastern Shandong Province, China: Spatio-temporal distribution, sensitivity regimes, and sources. *J. Environ. Chem. Eng.*, 13, 117389. https://doi.org/10.1016/j.jece.2025.117389.

Liu Y, Wang T, 2020. Worsening urban ozone pollution in China from 2013 to 2017-Part 1: The complex and varying roles of meteorology. *Atmos. Chem. Phys.*, 20, 6305–6321. https://doi.org/10.5194/acp-20-6305-2020.

Lundberg SM, Lee SI, 2017. A unified approach to interpreting model predictions. *Adv. Neural Inf. Process. Syst.*, 30, 4768–4777. https://doi.org/10.48550/arXiv.1705.07874.

Lundberg SM, Erion G, Chen H, et al., 2020. From local explanations to global understanding with explainable AI for trees. *Nat. Mach. Intell.*, 2, 56–67. https://doi.org/10.1038/s42256-019-0138-9.

Madukpe VN, Ugoala CB, Nnadi N, et al., 2025. A topological approach in analyzing the shifts in air pollutants' dynamics pre- and post-COVID-19 lockdown era. *Environ. Monit. Assess.*, 197, 719. https://doi.org/10.1007/s10661-025-14159-3.

Mangalathu S, Hwang SH, Jeon JS, 2020. Failure mode and effects analysis of RC members based on machine-learning-based SHapley Additive exPlanations (SHAP) approach. *Eng. Struct.*, 219, 110927. https://doi.org/10.1016/j.engstruct.2020.110927.

Merico E, Grasso FM, Cesari D, et al., 2020. Characterisation of atmospheric pollution near an industrial site with a biogas production and combustion plant in southern Italy. *Sci. Total Environ.*, 717, 137220. https://doi.org/10.1016/j.scitotenv.2020.137220.

Ministry of Ecology and Environment of the People's Republic of China (MEE), 2024. Ministry of ecology and environment releases national ambient air quality status for December 2023 and January–December 2023. https://www.mee.gov.cn/ywdt/xwfb/202401/t20240125_1064784.shtml (accessed January 25 2024).

Ministry of Transport of the People's Republic of China (MOT), 2024. 2023 national port cargo and container throughput. https://xxgk.mot.gov.cn/2020/jigou/zhghs/202404/t20240416_4128399.html (accessed April 16, 2024).

Nizamani MM, Zhang HL, Bolan N, et al., 2024. Understanding the drivers of $PM_{2.5}$ concentrations in Chinese cities: A comprehensive study of anthropogenic and environmental factors. *Environ. Pollut.*, 361, 124783. https://doi.org/10.1016/j.envpol.2024.124783.

Pendergrass D, Jacob D, Oak Y, et al., 2025. Wintertime trends of fine particulate matter ($PM_{2.5}$) in South Korea, 2012–2022: response of nitrate and organic components to decreasing NO_x emissions. *Geophys. Res. Lett.*, 52, e2025GL116091. https://doi.org/10.1029/2025GL116091.

Shandong Provincial Bureau of Statistics (SDBS), 2024. 2024 Shandong statistical yearbook. http://tjj.shandong.gov.cn/tjnj/nj2024/zk/indexch.htm (accessed December 28, 2024).

Shandong Provincial People's Government (SPPG), 2024a. Air Quality Status and Dust Fall Monitoring results for January to December 2023 in the province. http://www.shandong.gov.cn/art/2024/1/29/art_305267_

10347461.html?xxgkhide=1 (accessed January 29 2024).

Shandong Provincial People's Government (SPPG), 2024b. 2023 Shandong Province Ecological Environment Status Bulletin. http://xxgk.sdein.gov.cn/wryhjjgxxgk/zlkz/zkgb/202406/P020240606454202370719.pdf (accessed June 6, 2024).

Shen Y, Zhang L, Fang X, et al., 2019. Spatiotemporal patterns of recent $PM_{2.5}$ concentrations over typical urban agglomerations in China. *Sci. Total Environ.*, 655, 13–26. https://doi.org/10.1016/j.scitotenv.2018.11.105.

Shi Z, Song C, Liu B, et al., 2021. Abrupt but smaller than expected changes in surface air quality attributable to COVID-19 lockdowns. *Sci. Adv.*, 7, 3. https://doi.org/10.1126/sciadv.abd6696.

Song C, Liu B, Cheng K, et al., 2023. Attribution of air quality benefits to clean winter heating policies in China: Combining machine learning with causal inference. *Environ. Sci. Technol.*, 57, 17707–17717. https://pubs.acs.org/doi/10.1021/acs.est.2c06800.

Song Q, Huang L, Zhang Y, et al., 2025. Driving factors of $PM_{2.5}$ pollution rebound in north China plain in early 2023. Environ. *Sci. Technol. Lett.*, 12, 305–312. https://doi.org/10.1021/acs.estlett.4c01153.

Wang G, Qian Y, Kong F, et al., 2023. Non-methane hydrocarbon characteristics and their ozone and secondary organic aerosol formation potentials and sources in the plate and logistics capital of China. *Atmos. Pollut. Res.*, 14, 101873. https://doi.org/10.1016/j.apr.2023.101873.

Wang G, Yang X, Liu S, et al., 2025. Unveiling the drivers of $PM_{2.5}$ pollution in an industrial inland city in China during heating seasons (2021–2024) by an integrated machine learning method. *J. Hazard. Mater.*, 500, 140495. https://doi.org/10.1016/j.jhazmat.2025.140495.

Wen Z, Ma X, Xu W, et al., 2024. Combined short-term and long-term emission controls improve air quality sustainably in China. *Nat. Commun.*, 15, 5169. https://doi.org/10.1038/s41467-024-49539-9.

Wu K, Zhu S, Mac Kinnon M, et al., 2023. Unexpected deterioration of O_3 pollution in the South Coast Air Basin of California: The role of meteorology and emissions. *Environ. Pollut.*, 330, 121728. https://doi.org/10.1016/j.envpol.2023.121728.

Xiao Q, Zheng Y, Geng GN, et al., 2021. Separating emission and meteorological contribution to $PM_{2.5}$ trends over East China during 2000–2018. *Atmos. Chem. Phys.*, 21, 9475–9496. https://doi.org/10.5194/acp-21-9475-2021.

Xu Q, Wang S, Jiang J, et al., 2019. Nitrate dominates the chemical composition of $PM_{2.5}$ during haze event in Beijing, China. Sci. Total Environ. 2019, 689, 1293–1303. https://doi.org/10.1016/j.scitotenv.2019.06.294.

Yao S, Fan F, Jia H, et al., 2025a. Quantitative impacts of VOC sources on atmospheric oxidation capacity and O_3 formation from a megacity in China. *Atmos. Environ.*, 344, 121033. https://doi.org/10.1016/j.atmosenv.2025.121033.

Yao S, Jia H, Fan F, et al., 2025b. Assessing ozone formation impact through SHAP interaction redistribution analysis: A novel framework for evaluating VOC photochemical loss and source interactions. *Environ. Impact Asses.*, 115, 108017. https://doi.org/10.1016/j.eiar.2025.108017.

Zhang H, Guo W, Wang J, et al., 2025a. Scenario-dependent O_3 driver identification and formation responses to VOCs/NO_x emission reduction pathways from integrated and sectoral sources in the Beijing-Tianjin-Hebei region, China. *J. Hazard. Mater.*, 496, 139468. https://doi.org/10.1016/j.jhazmat.2025.139468.

Zhang K, Chen Q, Hong Y, et al., 2025b. Elucidating contributions of meteorology and emissions to O_3 variations in coastal city of China during 2019–2022: Insights from VOCs sources. *Environ. Pollut.*, 366, 125491. https://doi.org/10.1016/j.envpol.2024.125491.

Zhang Q, Zheng Y, Tong D, et al., 2019. Drivers of improved $PM_{2.5}$ air quality in China from 2013 to 2017. *Natl. Acad. Sci. U.S.A.*, 116, 24463–24469. https://doi.org/10.1073/pnas.1907956116.

Zhang W, Xu Q, Gao L, et al., 2025c. ITSC fault diagnosis for PMSM by using adaptive filtering and tree-structured parzen estimator optimized-automated random forest. *Electr. Eng.*, 107, 4711–4725. https://doi.org/10.1007/s00202-024-02788-9.

Zhang Z, Wang S, Wang P, et al., 2024. Regional transport dominates air pollution events in all seasons in Beijing in 2020. *Atmos. Environ.*, 323, 120395. https://doi.org/10.1016/j.atmosenv.2024.120395.

Zhao N, Zhang H, Wang G, et al., 2025. Revealing the nonlinear responses of $PM_{2.5}$ and O_3 to VOC and NO_x emissions from various sources in Shandong, China. *J. Hazard. Mater.*, 489, 137655. https://doi.org/10.1016/j.jhazmat.2025.137655.

Electronic supplementary materials

Texts S1-S3, Tables S1-S6, Fig. S1

中文概要

题　目：基于集成机器学习方法揭示 2023 年山东省三个时期 $PM_{2.5}$ 和 O_3 污染反弹的驱动因素

作　者：王刚[1]，刘赛[1]，王凯[2,3]，孟慧娟[4]，赵娜[5]，张晗宇[6]

机　构：[1]中国石油大学（华东），化学与化工学院环境与安全工程系，中国青岛，266580；[2]山东省生态环境规划研究院，中国济南，250101；[3]生态环境部陆海统筹生态治理与系统调控重点实验室，中国济南，250101；[4]济南工程职业技术学院实训管理中心，中国济南，250200；[5]山东大学环境研究院，中国青岛，

266237；[6]北京工商大学,轻工科学与工程学院环境科学与工程系，中国北京，100048

目　的：2023 年，随着新冠疫情防控措施调整与经济全面复苏，山东省空气质量指数出现 4.3%的反弹，细颗粒物（$PM_{2.5}$）和臭氧（O_3）浓度均呈显著上升趋势。为揭示此次污染反弹的驱动机制，本文旨在量化人为排放与气象条件在不同季节对 $PM_{2.5}$ 和 O_3 反弹的贡献，识别主导因素，从而为后疫情时代制定差异化的空气质量管理策略提供科学依据。

创新点：1. 分时段污染驱动因素解析：针对 $PM_{2.5}$（早春与秋收期）和 O_3（光化学季）分别定义了三个关键污染期，开展分时段的驱动因素分析，以揭示不同季节主导污染物的形成机制差异；2. 可解释机器学习框架构建：构建了基于树结构帕曾估计器（TPE）优化的随机森林-沙普利可加解释（RF-SHAP）集成学习框架，显著增强了模型对非线性关系的拟合能力，并实现了预测结果的可解释性。

方　法：1. 分时段预测模型构建：采用 TPE 对随机森林（RF）模型进行超参数优化，分别针对各关键污染期（$PM_{2.5}$ 污染期与 O_3 光化学季）建立预测模型。将数据集按 80%训练集、20%测试集划分，并评估模型性能；2. 特征贡献解释：基于训练好的 RF 模型，运用 SHAP 算法计算各特征变量（以时间变量作为人为排放活动水平的代理变量，结合气象变量）对预测结果的边际贡献值；3. 气象与排放贡献分离：采用“去气象”方法（重复进行 1000 次随机采样预测，每次随机打乱气象变量顺序以重构气象无影响情景），定量分离人为排放与气象因素对污染浓度的相对贡献；4. 多维度验证：结合 MEIC 排放清单、卫星火点数据、典型城市（临沂）的 $PM_{2.5}$ 化学组分及 VOCs 离线采样分析结果，从排放源、火点活动、化学组成等多角度验证关键污染期的驱动机制一致性。

结　论：1. $PM_{2.5}$ 污染反弹以人为排放主导：早春期（2~4 月）人为排放贡献 14.1%，秋收期（9~10 月）贡献 19.0%。主要驱动因素为工业活动恢复（能源消费增长 9.2%）与秸秆焚烧增加（火点数量上升 70.0%）；2. O_3 污染反弹受气象影响更显著：气象条件的贡献（5.8%）高于人为排放（3.3%）。关键气象因子包括大气氧化能力增强、总云量减少及边界层高度变化；但交通和石化行业的前体物排放仍是 O3 生成的物质基础；3. 温度升高促进二次无机气溶胶生成：升温加速了 SO_2 的液相氧化过程，并推动 NH_4NO_3 热平衡向颗粒相移动，从而强化二次无机气溶胶的形成；4. 建议实施季节性差异化管控策略：春秋季应重点削减工业与农业源排放以控制 $PM_{2.5}$，夏季则需结合气象监测，加强对 NO_x 和 VOCs 等前体物的排放控制，以抑制 O_3 生成。

关键词：空气污染反弹；驱动因素；RF-SHAP；人为排放；气象条件